Investigating the repair of alveolar bone defects by gelatin methacrylate hydrogels-encapsulated human periodontal ligament stem cells

Pan, Jie

2020

Pan , J , Deng , J , Yu , L , Wang , Y , Zhang , W , Han , X , Camargo , P H C , Wang , J & Liu , Y 2020 , ' Investigating the repair of alveolar bone defects by gelatin methacrylate hydrogels-encapsulated human periodontal ligament stem cells ' , Journal of Materials Science: Materials in Medicine , vol. 31 , no. 1 , 3 . https://doi.org/10.1007/s10856-019-6333-8

http://hdl.handle.net/10138/326485
https://doi.org/10.1007/s10856-019-6333-8

Journal of Materials Science: Materials in Medicine (2020) 31:3
https://doi.org/10.1007/s10856-019-6333-8

TISSUE ENGINEERING CONSTRUCTS AND CELL SUBSTRATES

Original Research

Investigating the repair of alveolar bone defects by gelatin methacrylate hydrogels-encapsulated human periodontal ligament stem cells

Jie Pan[1,2] · Jiajia Deng[1,2] · Liming Yu[1,2] · Yuhui Wang[1,2] · Weihua Zhang[1,2] · Xinxin Han[1,2] · Pedro H. C. Camargo[3,4] · Jiale Wang[5,6] · Yuehua Liu[1,2]

Received: 22 May 2019 / Accepted: 16 November 2019 / Published online: 5 December 2019

Abstract

Although various efforts have been made to develop effective treatments for alveolar bone defect, alveolar regeneration has been emerging as the one with the most potential Herein, we investigated the potential of gelatin methacrylate (GelMA) hydrogels-encapsulated human periodontal ligament stem cells (hPDLSCs) to regenerate alveolar bone. The easy, rapid, and cost-effective nature of GelMA hydrogels makes them a promising mode of stem cell-delivery for clinically relevant alveolar bone regeneration. More importantly, GelMA hydrogels provide an optimal niche for hPDLSCs proliferation, migration and osteogenic differentiation, which are critical for alveolar bone regeneration. In this study, we examined the microstructure of GelMA hydrogels, and identified a highly porous and interconnected network. Compressive test of GelMA hydrogels showed that the stress reached a maximum value of 13.67 ± 0.03 kPa when the strain reached 55%. The maximum values of swelling ratio were 700 ± 47% at the fifth hour. The proliferation rate of hPDLSCs in the GelMA hydrogels resembled that in 2D culture and gradually increased. We established a critical-sized rat model of alveolar bone defects, and applied Micro-CT to assess new bone formation. Compared to the control group, there was substantial bone regeneration in the GelMA + hPDLSCs group at both 4 and 8 weeks after the operation. Histological analysis results were consistent with Micro-CT results. Our study demonstrates that the GelMA hydrogels-encapsulated hPDLSCs have a significant alveolar regenerative potential, and may represent a new strategy for the therapy of alveolar bone defects.

These authors contributed equally: Jie Pan, Jiajia Deng

✉ Jiale Wang
jiale.wang@dhu.edu.cn

✉ Yuehua Liu
liuyuehua@fudan.edu.cn

[1] Department of Orthodontics, Shanghai Stomatological Hospital, Fudan University, Shanghai 200001, PR China

[2] Oral Biomedical Engineering Laboratory, Shanghai Stomatological Hospital, Fudan University, Shanghai 200001, PR China

[3] Department of Chemistry, University of Helsinki, A.I. Virtasen aukio 1, FI 00014 Helsinki, Finland

[4] Departamento de Química Fundamental, Instituto de Química, Universidade de São Paulo, Av. Prof. Lineu Prestes, 748, São Paulo, SP 05508-000, Brazil

[5] College of Science, Donghua University, Shanghai 201620, China

[6] Shanghai Institute of Intelligent Electronics and Systems, Donghua University, Shanghai 201620, China

Graphical Abstract

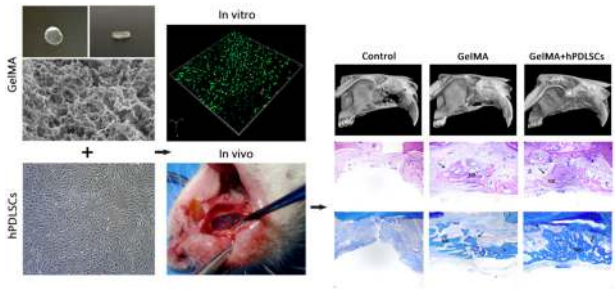

1 Introduction

Alveolar bone deficiencies can result from periodontal disease, trauma, infection, congenital alveolar fenestration, and so on [1]. Various agents, such as anti-inflammatory drugs, systemic antibiotics, bisphosphonates, etc., have been used to promote alveolar bone formation [2, 3]. However, the results have been discouraging. Recently, stem cell therapy has been garnering attention in facilitating alveolar bone regeneration [4, 5] as some studies have indicated that different types of pluripotent mesenchymal stromal cells (MSCs) can be used for the regeneration of periodontal tissues [6–8]. Seo et al. showed that human periodontal ligament stem cells (hPDLSCs) displayed a higher level of proliferation and osteogenic differentiation capability than bone mesenchymal stromal cells (BMSCs) [9]. These data suggest that hPDLSCs could be used as a potential therapy for regeneration of periodontal bone tissues in alveolar bone deficiencies.

Although hPDLSCs are ideal therapeutic candidates for the regeneration of periodontal bone tissues, the mode of delivery of these stem cells still needs to be perfected. While optimizing the delivery of hPDLSCs can result in higher quality tissue regeneration, the process still remains challenging. Test of various biomaterials for 3D delivery of stem cells has demonstrated an important role of vehicle in the performance of encapsulated cells as well as the success of the regenerative therapy [10, 11]. Among these biomaterials, gelatin methacrylate (GelMA) hydrogels, which can retain cell-binding and are mechanically robust, represent a promising vehicle for stem cells delivery [12, 13]. Furthermore, their adjustable physicochemical properties makes GelMA hydrogels widely applicable in promoting high-quality tissue regeneration [12–16]. Since alveolar bone defects can be irregular in shapes, injecting liquid GelMA hydrogels can fill these irregularities quickly and effectively. GelMA hydrogels possess not only biocompatible and biodegradable properties, but are also cost-effective, non-cytotoxic and non-immunogenic, making them an ideal biological scaffold material. Furthermore, encapsulated cells retain excellent viability within GelMA hydrogels [17]. Therefore, we anticipate that due to their simple and cost-effective nature, GelMA hydrogels make an attractive biological scaffold to use for alveolar bone regeneration in clinic.

In this study, we investigated the use of GelMA hydrogels-encapsulated hPDLSCs to treat irregular alveolar bone defects. Remarkably, our data demonstrated that GelMA hydrogels-encapsulated hPDLSCs have a significant alveolar regenerative potential and may provide a new therapeutic strategy to treat alveolar bone defects.

2 Materials and methods

2.1 GelMA hydrogels preparation and characterization

GelMA was prepared as reported previously [16, 18]. In brief, gelatin type A was mixed with phosphate-buffered saline (PBS) at a ratio of 10% (w/v), and heated to 50 °C, while continuously stirring at 50 °C for 3 h. After adding an equal volume of PBS, the solution was then dialyzed with a 0.22 μm membrane using deionized (DI) H_2O at 37 °C for 7 days. The samples were frozen and stored in the dark.

10% (w/v) GelMA solution was made by dissolving the freeze-dried GelMA. Meanwhile, blue light photoinitiator, lithium phenyl-2,4,6trimethylbenzoylphosphinate (LAP), was synthesized [19] and added to the prepolymer solution at 0.5% (w/v) concentration. Finally, the GelMA hydrogels were exposed to LAP blue light (405 nm, UltraFire, WF-501B) for 5 s.

The structure and pore size of the freeze-dried GelMA samples were imaged using a scanning electron microscopy (SEM) (S-3400N, HITACHI, Japan). The average pore sizes of the scaffolds were then measured by using ImageJ 1.50 software and taking multiple measurements. GelMA samples for the compressive test were prepared inside a PDMS mold (diameter = 10 mm; height = 10 mm, $n = 3$) and soaked in PBS at 37 °C. After 24 h, the compressive

stress-strain curve was obtained by testing GelMA samples at a consistent compression speed (1 mm/min). GelMA's swelling ratio was then derived from the curve. The GelMA samples were prepared inside a PDMS mold (diameter = 10 mm; height = 1 mm, $n = 3$) and then lyophilized. The samples were then weighed, and placed in PBS solution (pH = 7.4) at 37 °C for 1, 2, 3, 4, and 5 h. At each specified time, samples were weighed and the swelling ratios of GelMA samples were calculated by (wet weight − dry weight)/dry weight × 100%.

2.2 hPDLSCs isolation and characterization

2.2.1 hPDLSCs isolation and culture

Extracted human teeth (for clinically relevant reasons from Shanghai Stomatological Hospital), were collected, after approval by the Ethics Committee of Shanghai Stomatological Hospital. The hPDLSCs were harvested from the extracted teeth as mentioned before [20]. Briefly, periodontal ligament tissues were scraped from the middle of the tooth-root surfaces and cut into small fragments. The fragments were then placed onto a 100-mm dish, cultured in minimum essential alpha medium (α-MEM), containing 10% fetal bovine serum (FBS) and 1% penicillin-streptomycin. The media was changed every 3 days. Finally, hPDLSCs were harvested to generate single cell clones.

Cell proliferation was measured by a Cell Counting Kit-8 (CCK-8) test at 1, 3, 5, and 7 days after culture. 100 µL supernatant with the cells was transferred into 96-well culture plates and then incubated with CCK-8 (1:10) for 2 h. The absorbance of the solution was then tested by a microplate reader (Epoch2, Biotek, USA) at 450 nm.

2.2.2 Immunofluorescence staining

Samples were grown on 24-well culture plates and then fixed in a 4% paraformaldehyde solution for 20 min, followed by 3 washes with PBS. The hPDLSCs were permeabilized with 0.25% Triton X-100 for 10 min, and then blocked in 5% BSA for 1 h. The cells were then incubated with mouse anti-human Stro-1 antibody (1:1000, NBP1-48356, NOVUS) and CD146 (1:1000, NBP2-44510, NOVUS).

2.2.3 Alizarin red staining and oil red staining

The hPDLSCs from passage 3 were cultured in 6-well plates. At 80% confluence, the media was replaced with the osteogenic medium, composed of α-MEM, 10% FBS, 10 mmol/L β-glycerophosphate, 50 mg/L L-ascorbic acid and 0.1 µmol/L Dexamethasone, and was changed every 3 days. Adipogenic medium composed of α-MEM, 10% FBS, 10 µmol/L dexamethasone, 200 µmol/L Indomethacin, 10 mg/mL insulin and 0.5 mM 3-isobutyl-1-methyl-xanthine (IBMX). After 21 days of culture in adipogenic medium, the cells were fixed in 4% paraformaldehyde for 20 min at room temperature and then washed with PBS 3 times. All samples were soaked in 0.1% Alizarin Red S (ARS) (pH = 8.3) and Oil Red O solution for 20 min, washed 3 times with PBS, and finally dried at room temperature. The images were obtained using a microscope (Leica, S/N 477892, Germany).

2.3 hPDLSCs capsulation and 3D culture

A total of 1×10^6 hPDLSCs were resuspended in 1 ml 10% (w/v) GelMA hydrogels. Then GelMA hydrogels were exposed to LAP 405 nm blue light for 5 s. hPDLSC entrapped within the microgel units were cultured at 37 °C with 5% CO_2. The culture medium was changed every 3 days.

2.4 Live-dead and cell proliferation assays in GelMA hydrogels

Encapsulated hPDLSCs were washed 3 times with PBS and labeled with Calcein-AM/ethidium (CalceinAM/PI, Invitrogen) at 37 °C for 30 mins. After 3 PBS washes, the labeled cells were visualized with a fluorescence microscope (Leica, S/N 477892, Germany). Cell proliferation was tested with CCK-8 at days 1, 3, 5 and 7 respectively. The cells were incubated in medium containing 10% CCK-8 solution for 2 h at 37 °C, 5% CO_2 in the dark. A 100 µL supernatant was added into 96-well culture plates, and absorbance measured by a microplate reader at 450 nm. Wells with the same medium, but lacking cells, were used as blank controls.

2.5 Experimental model

Our study was conducted conforming to Fudan University Animal laboratory guidelines. 8-week-old Sprague-Dawley rats were purchased from Beijing Vital River Laboratory Animal Technology limited-liability company (Beijing, China). Rats were raised in a constant temperature (22 ± 1 °C) environment. Critical size alveolar bone defects were established as mentioned previously [21–23]. Briefly, all rats were first anesthetized with 2% pentobarbital sodium (0.3 ml/100 g, given intraperitoneally) prior to the surgical procedure. Rats were placed in a supine position with the mandible and tongue retracted. A 1-cm longitudinal incision between the alveolar mucosa and hard palate was then made using a

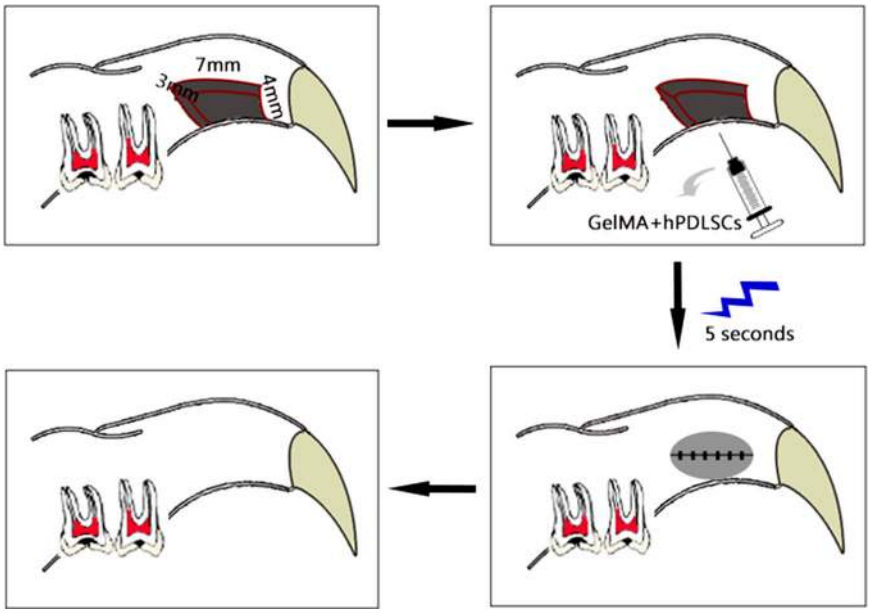

Fig. 1 Representative illustration of the steps for performing the bone defect

No. 11 blade scalpel. In order to clearly reveal the alveolar bone, a dentoalveolar periosteum was performed to elevate it. Using a hand-operated low-speed grinder and a side-cutting bit, a $7 \times 4 \times 3\ mm^3$ alveolar defect was then established. The alveolar bone defect was measured with a vernier caliper and validated by a master template to ensure authenticity. Rats were randomized into 3 groups: a control untreated group; a GelMA group in which the alveolar bone defect was injected with GelMA hydrogels alone; a GelMA + hPDLSCs group in which the defect was injected with GelMA hydrogels-encapsulated hPDLSCs (1×10^6 cells/mL). After surgery, the gingival mucosa was seamed appropriately with 5-0 Vicryl suture (Fig. 1). All rats were fed with soft food for 3 days and then fed regular diet there after. At 4 and 8 weeks after surgery, rats were sacrificed, and alveolar specimens were harvested.

2.6 Morphometric analysis with micro-computed tomography (Micro-CT)

All rats were sacrificed at 4 and 8 weeks and samples were scanned by a conical beam microcomputed tomography scanner (Sky-Scan 1076; Bruker-micro CT, Kontich, Belgium) using following exposure parameters: 0.24 s, 40 kV and 250 µA. Serial 18-µm-thick coronal sections of the labial surface of the maxillary incisors to the zygomatic arch were obtained. The serial sections were reconstructed into a three-dimensional image using reconstructions and osteogenic parameters conducted with NRecon v.1.6.9 software. The osteogenic parameters such as tissue volume (TV), bone volume (BV), and the ratio of BV/TV, were measured by three observers who were blinded to the experimental design of the trials.

2.7 Histological analysis

After the Micro-CT scan, samples from each group were decalcified. The decalcifying fluid was replaced every 3 days until there was no resistance to pinprick. The samples were dehydrated through graded ethanol from 75 to 100% and then embedded in paraffin after decalcification. A consecutive 6 µm sagittal sections were obtained for each specimen. Sections from the embedded specimen were stained with hematoxylin and eosin (H&E) and Masson's trichrome stain to evaluate the alveolar bone formation. Immunohistochemical staining of Alkaline phosphatase (ALP, Abcam, ab95462) was used to observe the ALP activity. A dark brown color represented positive ALP staining.

2.8 Statistical analysis

Statistical differences ($p < 0.05$) between different groups were analyzed. The analysis was done using a SAS 6.12 statistical software package. All data were shown as mean ± standard deviation.

3 Results

3.1 Preparation and characterization of hPDLSCs

After 14 days of primary culture and normal passaging, we isolated hPDLSCs and successfully passaged (Fig. 2a). The hPDLSCs proliferated significantly more with time, with no significant difference among the three passages. We then spread 200 cells on a 100-mm dish to allow formation of

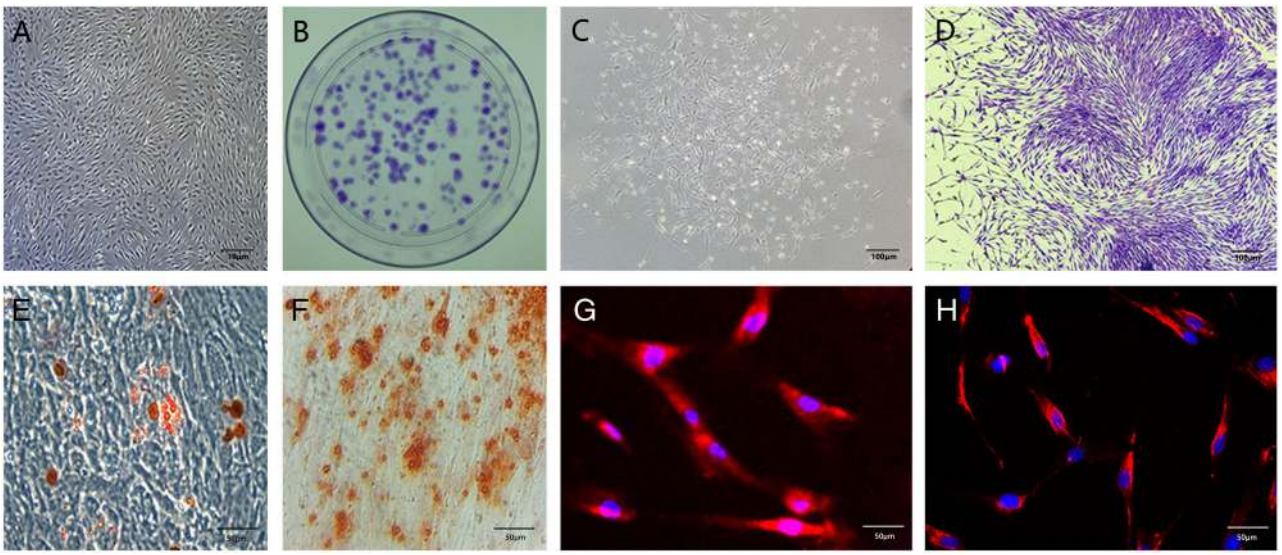

Fig. 2 Important features of hPDLSCs. **a** The morphology of hPDLSCs was typical of spindle shaped cells like fibroblast in the microscopic field of view. **b** Single colonies formed after seeding 200 cells and culturing for 10 days with crystal violet staining. **c** Cell clusters were derived from hPDLSCs consistent with typical fibroblast-like cells. **d** Cell clusters were stained with Crystal Violet in the microscopic view. **e** Lipid droplets formed after adipogenic induction for 3 weeks, and stained with Oil Red O staining. **f** Mineralized nodules were formed after osteogenic induction for 3 weeks with Alizarin Red staining. **g** CD146 expression of hPDLSCs shown with immunofluorescence staining. **h** Stro-1 expression of hPDLSCs shown with immunofluorescence staining

single cell colonies. The cells were cultured for 10 days, and stained with Crystal Violet to identify single colonies (Fig. 2b). The morphology of cell clusters derived from hPDLSCs was typical of fibroblasts, under the high-power field of view (Fig. 2b–d). After osteogenic induction in vitro, the cells were stained with Alizarin-red stain, which indicated progressive increase in extracellular mineralization (Fig. 2e). The lipid droplets in hPDLSCs could be detected with oil red staining after adipogenic was induced (Fig. 2f). Immunofluorescence staining showed that the hPDLSCs were positive for stem cells specific markers, such as Stro-1 and CD146 (Fig. 2g, h, respectively).

3.2 Characteristics of GelMA hydrogels and viability of encapsulated hPDLSCs in vitro

Figure 3a illustrates the formation process of GelMA hydrogels. Figure 3b, c shows the macrostructure and microstructure of GelMA hydrogels. As can be seen, the pore size of the GelMA hydrogels was 46.43 ± 12.65 μm. To assess the mechanical properties of 10% (w/v) GelMA hydrogels, a compressive test was conducted on samples. From the compressive stress-strain curves, we found that the stress reached a maximum value of 13.67 ± 0.03 kPa when the strain reached 55% (Fig. 3d and Table 1). We also calculated 10% (w/v) GelMA hydrogels' swelling ratio. The swelling ratio is an important parameter of a cell/drug carrier due to its crucial effects on cellular metabolism and release rate. As shown in Fig. 3e and Table 1, the swelling ratio of GelMA hydrogels increased rapidly at first 1 h, reaching a maximum ratio of $700 \pm 47\%$ at the fifth hour. Additionally, the swelling was maintained around the equilibrium when all samples were soaked for 5 h.

In order to assess the viability of encapsulated hPDLSCs, live/dead staining and CCK-8 assay were applied. The hPDLSCs were encapsulated with the hydrogels at a 1×10^6 cells/mL density and the viability of hPDLSCs was measured at days 1, 3, 5 and 7, respectively. Live/dead staining results demonstrated high viability of encapsulated hPDLSCs, cultured in regular culture medium at all tested time intervals (Fig. 4a). The hPDLSCs grew well in the 10% (w/v) GelMA hydrogels, and interestingly, remained suspended in the gel space as spheres after 1 day of culture. After the hPDLSCs stretched and grew in the gel, the cells were still in a good growth state (Fig. 4b). To capture cell growth, a 7d image of the hPDLSCs culture were taken by confocal laser (A1R, Nikon, Japan) after 7 days. The solution was changed every 3 days, and the Live/Dead staining reagent was used on the 7th day to identify the growth status of cells in 7d culture in the gel. Live cells are depicted by the green color (stained with calcein AM), dead cells are depicted with the red color (stained with EthD-1), and the nucleus is depicted by the blue color (stained with hochest33342) (Fig. 4c). There was a gradual increase in viability of cells capsulated in GelMA hydrogels over the 7 days of culture. We saw that the hPDLSCs in the GelMA hydrogels proliferated at a rate, comparable to that of 2D culture and gradually increased (Fig. 4a).

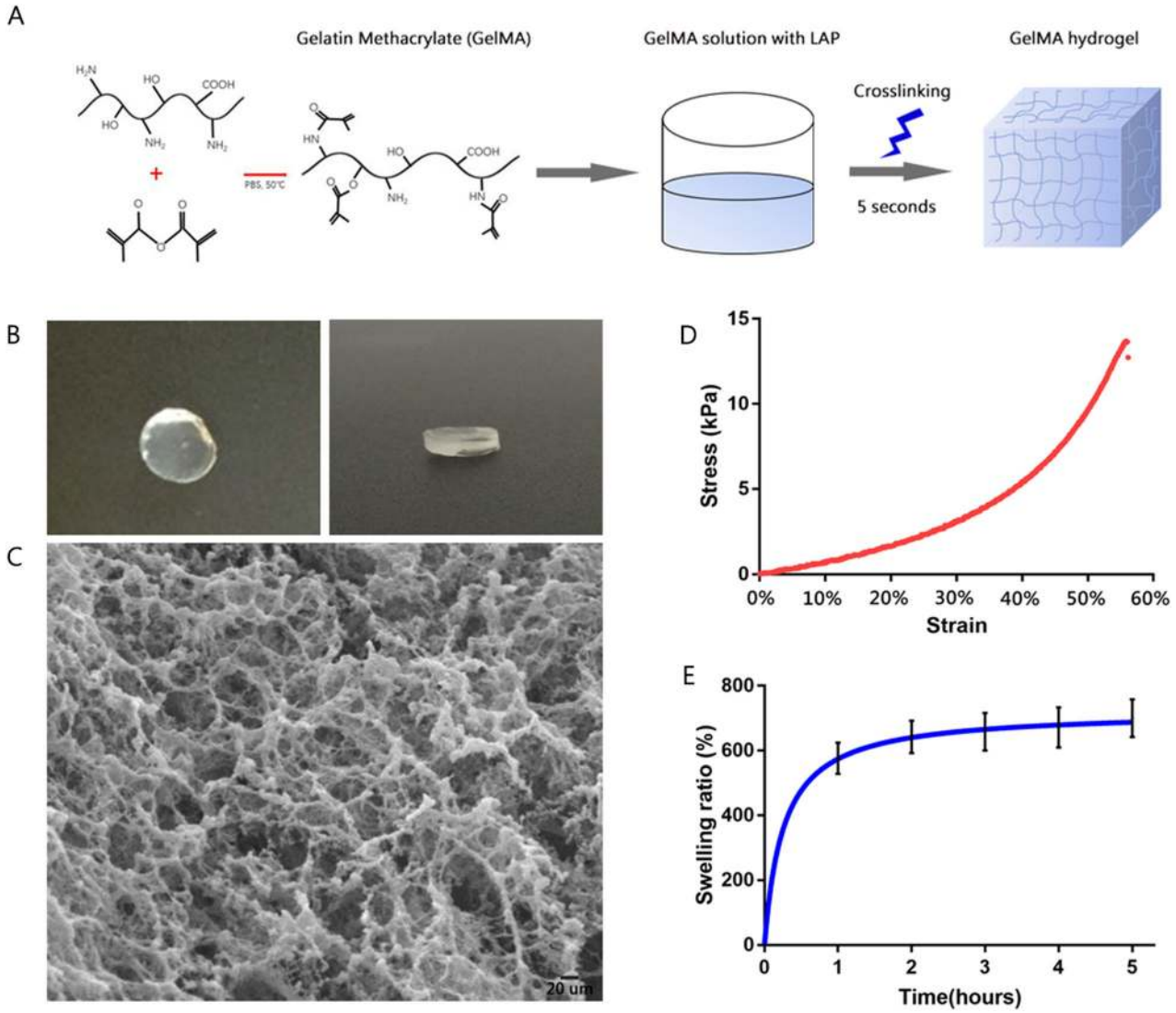

Fig. 3 Preparation and characterization of GelMA hydrogels. **a** Schematic illustration of GelMA hydrogels formation. **b**, **c** The macrostructure and microstructure of GelMA hydrogels were imaged. **d** Compressive stress–strain curves of GelMA hydrogel, the maximum value was 13.7 kPa when the strain reached 55%. **e** The highest adsorption capacity of GelMA hydrogels was 753% at the fifth h

3.3 GelMA hydrogels-encapsulated hPDLSCs enhance alveolar bone formation in vivo

3.3.1 Micro-CT analysis

We established rat critical size alveolar bone defects as mentioned before. Since liquid GelMA hydrogels fill irregular alveolar defects quickly and easily, we applied GelMA hydrogels to the bone defect (Fig. 5), and used Micro-CT to reconstruct 3D morphology of the repaired alveolar bone and thus assess new bone formation. In all groups (the control group, GelMA group, and GelMA + hPDLSCs group), new bone formed in the area surrounding the bone defect at 4 weeks after the operation. However, unlike in the control group, new bone also formed at the center of the bone defect in the GelMA group, and GelMA + hPDLSCs group. At 8 weeks after the operation, the newly formed bone tissues were both in the surrounding area and at the center of the bone defect. In particular, there was a substantial bone regeneration in the GelMA + hPDLSCs group at both 4 and 8 weeks after the operation. The bone formation was less pronounced in the GelMA group and least pronounced in the control group (Fig. 6a).

The quantity of new bone in the defect area was analyzed by using the above-mentioned osteogenic parameters (BV/TV) (Fig. 6b). Our data showed that 32.2, 39.4 and 58.8% of new bone regeneration was observed in the control group, GelMA group, and GelMA + hPDLSCs group, respectively, at 4 weeks after the operation. At 8 weeks after the operation, the bone regeneration values corresponded to 38.1, 51.4, and 67.2% in the Control group, GelMA group, and GelMA + hPDLSCs group, respectively. Therefore,

Table 1 Summary of physical properties of 10% (w/v) GelMA hydrogels

Compressive strength (kPa)	Elongation at break (%)	Swelling ratio (%)				
		1 h	2 h	3 h	4 h	5 h
13.67 ± 0.03	55 ± 5	576 ± 39	642 ± 41	658 ± 47	671 ± 51	700 ± 47

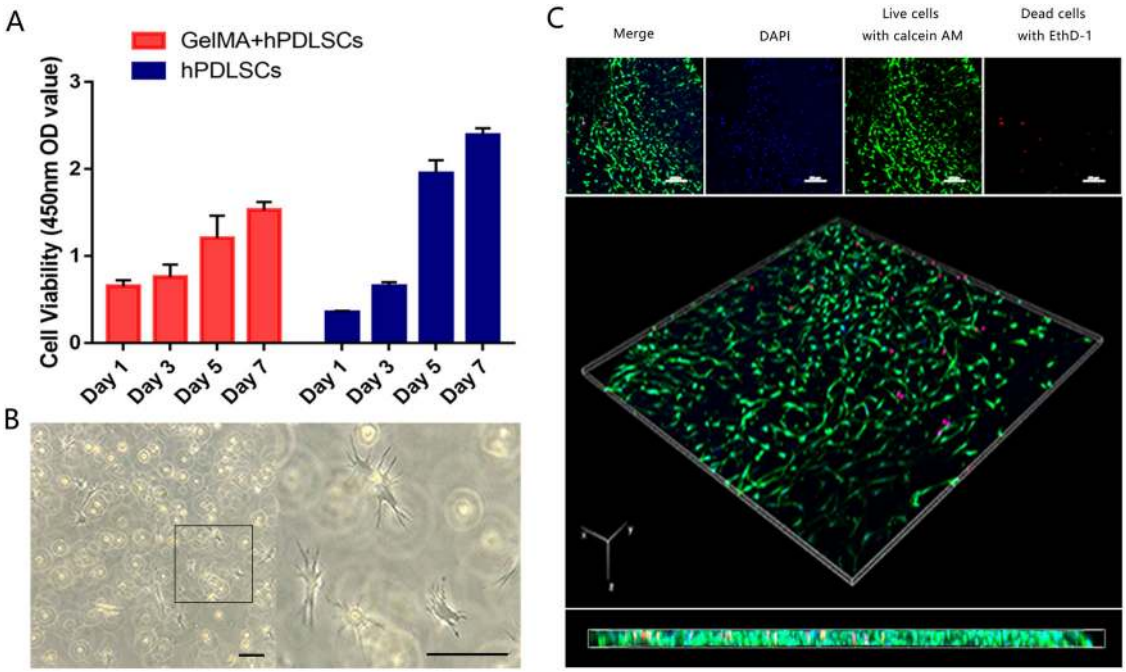

Fig. 4 Viability and proliferation of hPDLSCs in GelMA hydrogels. **a** CCK-8 method was used to assess cell viability by measuring the absorbance at 450 nm on the 1st, 3rd, 5th and 7th days after GelMA hydrogel formation. CCK-8 measurements revealed that there was a gradual increase in the cell viability over the 7 days of 2D (hPDLSCs) and 3D (GelMA + hPDLSCs) culture. **b** hPDLSCs were inoculated in gel for 24 h at a density of 1×10^6 /mL, where PDLSCs grew well, and remained suspended in gel space as spheres, bar = 100 um. **c** Live-Dead analysis of hPDLSCs in GleMA after 7 days is shown. The confocal laser microscope was used to take 7d pictures of the cell growth. The solution was changed every 3 days, and the Live/Dead staining reagent was used on the 7th day to identify the growth status of cells in 7d culture in the gel. Green represents living cells, red represents dead cells, and blue represents hochest 33342 staining nuclei

these observations indicate a significant variation of new bone formation among different groups.

3.3.2 Observation and analysis of histological sections

To validate new bone formation by histology, we performed histological analysis in sections at 8 weeks after the operation. Hematoxylin-eosin (HE) staining of the sections showed that there was substantial new bone formation in the defect area of GelMA + hPDLSCs group. The new bone formation in the defects was detectable to a lower degree in the GelMA group (Fig. 7a). Similarly, the results of Masson's trichrome staining demonstrated numerous fibrous tissues, with only minimal bone formation in the defect area of the control group but several areas of new bone formation in both GelMA and GelMA + hPDLSCs groups (Fig. 7b). Moreover, both mature and new bone was evident at higher magnification, and were found in the defect area of GelMA + hPDLSCs group. As expected, new bone formation in the defect area was low in the GelMA group and none in the control group (Fig. 7b). These results are consistent with Micro-CT results, suggesting efficient bone formation by GelMA + hPDLSCs. The results of the alkaline phosphatase activity (ALP activity) in the three groups are shown in Fig. 6c. Dark brown staining represents the presence of ALP. As shown in the figure, ALP activities were higher in the GelMA and GelMA + hPDLSCs groups than in the control group. Comparison between the GelMA and GelMA + hPDLSCs groups demonstrated a large amount of dark brown staining in the GelMA + hPDLSCs group compared to the GelMA group, suggesting higher ALP activity relative to the other samples. The average optical density (AOD) of the positive regions in the 3 groups were in agreement with the reported behavior for the groups, as shown in Fig. 7d. Overall, our results suggest that the GelMA hydrogels have a greater ability to repair alveolar bone defects, and this effect is further amplified when conjugated with hPDLSCs.

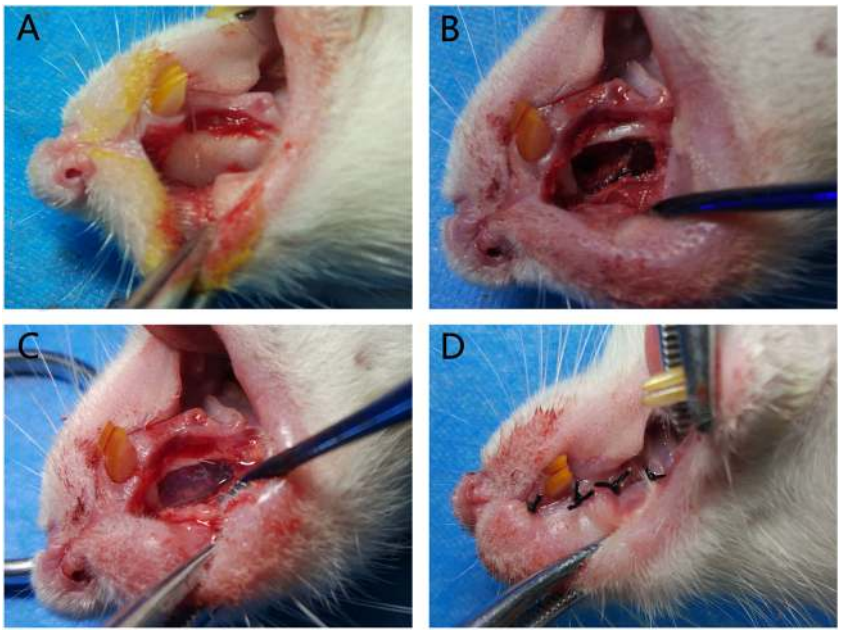

Fig. 5 The critical-size alveolar defects model. **a** Sprague-Dawley rats were placed in the supine position, and the dentoalveolar periosteum was elevated to reveal alveolar bone. **b** A $7 \times 4 \times 3\ mm^3$ defect was created. **c** The alveolar bone defect was filled with the GelMA hydrogels. **d** The mucosa was closed with an absorbable suture

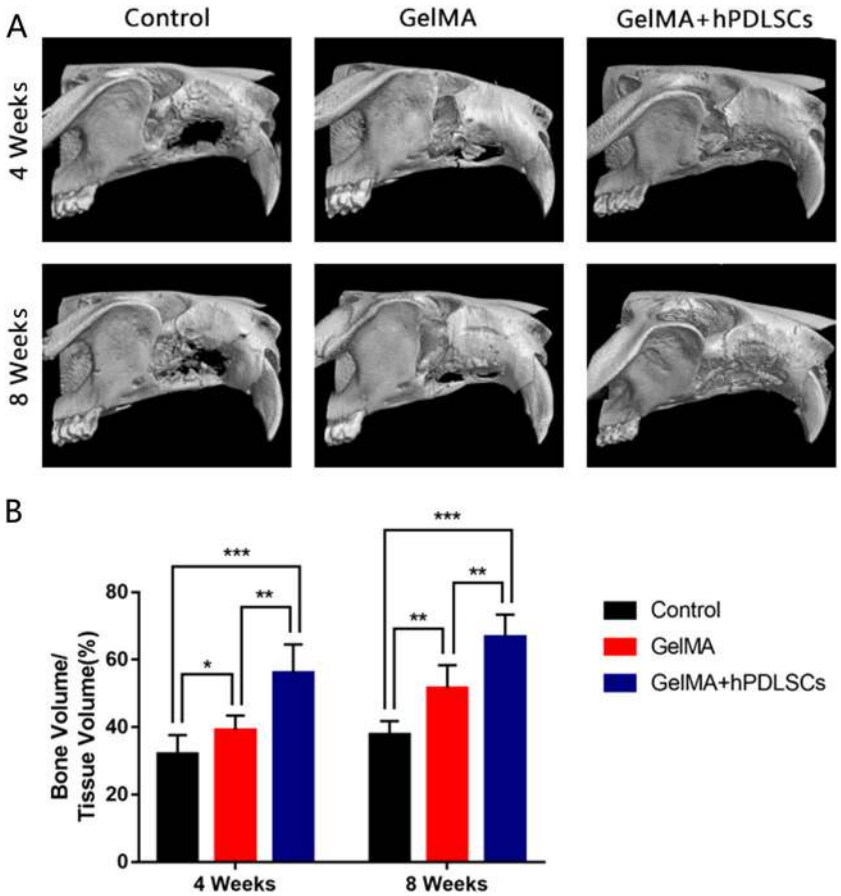

Fig. 6 Radiograph morphometric analysis of bone formation in alveolar defects. **a** Substantial new bone formation was observed in the defect area in GelMA + hPDLSCs group at both 4 and 8 weeks after operation. New bone formation was detected at a lower degree in GelMA group relative to GelMA + hPDLSCs, but still higher when compared to control group. **b** Statistically significant differences value of BV/TV in GelMA + hPDLSCs group relative to the control and GelMA groups at 4 and 8 weeks after operation ($^{*}P < 0.05$, $^{**}P < 0.01$, $^{***}P < 0.001$)

4 Discussion

Several studies have demonstrated that PDLSCs are highly proliferative and have better osteogenic capability than BMSCs [9]. The use of hPDLSCs for alveolar bone regeneration in previous studies demonstrated that hPDLSCs could differentiate into osteoblasts, form mineralized nodules, and promote bone regeneration [24, 25].

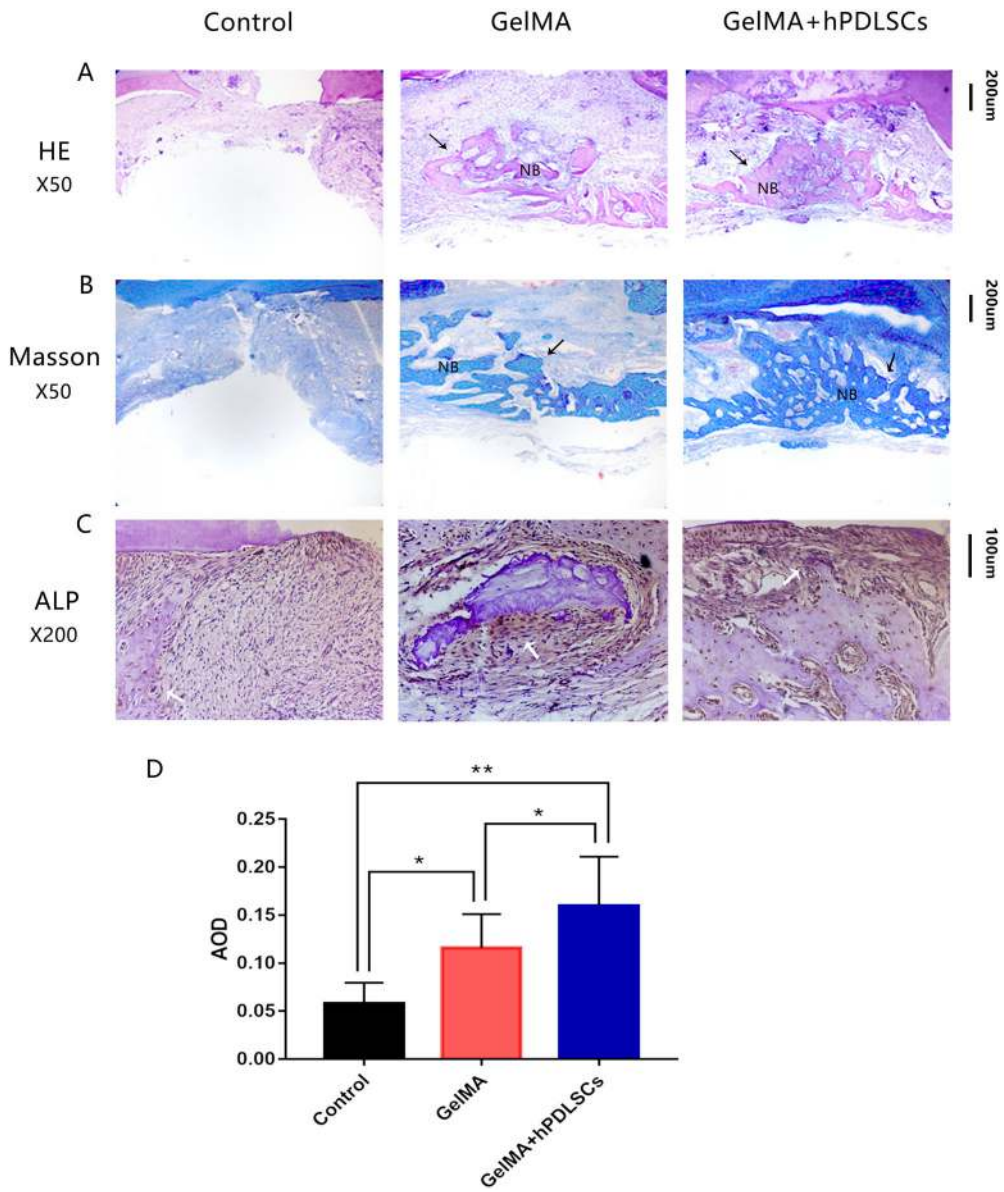

Fig. 7 Histological analysis of new bone formation at 8 weeks after operation. **a** H & E staining demonstrated substantial new bone formation in GelMA and GelMA + hPDLSCs groups, while limited new bone formation in the control group. **b** Masson's trichrome staining demonstrated much more new bone formation in GelMA + hPDLSCs group than in the GelMA group. Moreover, no bone formation in the defect area was detected in the control group. **c** Immunohistochemical staining of sections with anti-ALP antibody for all groups tested. The dark brown staining represents the presence of ALP. ALP activities were higher in the GelMA and GelMA + hPDLSCs groups relative to the control. **d** The bar-graph represents average optical density (AOD) of the ALP positive regions in the three groups. NB represents new bone. Black arrows indicate the newly formed bone tissue. White arrows indicate ALP positive regions ($^{*}P < 0.05$, $^{**}P < 0.01$)

Specifically, PDLSCs could generate a periodontal complex including alveolar bone, which can be a natural source of stem cells for alveolar bone formation. Allogeneic PDLSCs were also well tolerated in transplantation, and showed low immunogenicity [26]. We successfully isolated the hPDLSCs which showed typical spindle-shaped morphology. The adipogenic differentiation and osteogenic differentiation experiment confirmed that hPDLSCs isolated in our experiment showed multi-differentiation potential, which were similar to conventional stem cells. These reports, therefore, inspired us to use hPDLSCs and to test alveolar bone formation in rat alveolar bone defect model.

Despite these promising previous reports, it has been challenging to mimic the native extra-cellular matrix (ECM) niche of natural alveolar bone to guarantee the survival of the transplanted PDLSCs. Use of hydrogels have mitigated this challenge to a large extent. Hydrogels closely resemble the features of the ECM niche, as they can contribute to cell-matrix interactions, cell-cell interactions, proliferation, migration, and controlled differentiation [18, 27].

Furthermore, they also afford 3D supports for cell delivery and cellular growth in regenerative medicine [28]. Among the numerous hydrogels, GelMA hydrogels have unique and promising properties for tissue engineering [29]. Gelatin, derived from hydrolysis of collagen, is the main component of ECM that exists in many tissues, and can enhance cell attachment and cell remodeling, due to abundance of arginine-glycine-aspartic acid sequences and matrix metalloproteinase' target sequences [18, 30]. When cells suspended in GelMA prepolymer solutions are exposed to UV or blue light, the cell-laden 3D hydrogels form as a result of cross-linking. A widely used photoinitiator for cell encapsulation and tissue engineering is 2-hydroxy-4′-(2-hydroxyethoxy)-2-methylpropiophenone (Irgacure 2959). However, its use has been limited due to ultraviolet (UV) light (365 nm) exposure needed in the process [31]. Compared with Irgacure 2959, another photoinitiator, blue light photoinitiator LAP has higher water solubility, and can encapsulate cells at longer light wavelengths (405 nm) with lower photoinitiator concentrations, thereby facilitating efficient polymerization [19, 29]. Moreover, blue light is unlikely to lead to cell damage, and can transmit more reliably through tissues, which can further benefit to depth of cure [29]. To avoid UV light exposure that can have adverse consequences on the delivered cells and host tissues [29], we used blue light photoinitiator LAP (exposed to blue light (405 nm) for 5 s with GelMA hydrogels to encapsulate cells. Our results suggested that the cells were impervious to 5 s of blue light exposure, and showed high cell viability in the photocrosslinked cell-laden GelMA hydrogels (Fig. 4a, b).

The application of GelMA based scaffolds in the regeneration of loaded tissues, especially in the regeneration of skeletal muscle, bone tissues, and cartilage tissues, has witnessed great progress [18]. In the current study, we optimized the GelMA concentration to build scaffolds for application in bone tissue engineering. It has been reported that hydrogels with higher prepolymer concentrations display higher compressive modulus but lower bioactivity. In this regard, GelMA solutions in higher concentrations can enhance mechanical properties and osteogenic capabilities, and potentially also affect porosity, and cellular spreading and growth [32]. Although stem cells can exhibit better osteogenic differentiation at both 5 or 10% GelMA hydrogels, 10% GelMA hydrogels have been favored for osteogenic differentiation because of their compact hydrogel network and lower swelling properties [33]. 10% GelMA hydrogels also promote stem cells attachment, thus promoting better proliferation and differentiation [34]. As a result, considering both the activity and osteogenic differentiation capability of encapsulated hPDLSCs, we chose GelMA hydrogels with 10% prepolymer concentrations to encapsulate hPDLSCs.

Since liquid GelMA hydrogels can fill irregular alveolar defects quickly and easily, and allow hPDLSCs proliferation, the use of GelMA hydrogels-encapsulated hPDLSCs for therapy of alveolar bone defects is novel and promising. In Micro-CT analysis, we found that newly formed bone tissues in the GelMA + hPDLSCs group were significantly higher than in both the GelMA and control groups at both 4 and 8 weeks of post-surgery (Fig. 6a). Notably, the ratio of bone-volume-to-tissue-volume (BV/TV) in GelMA + hPDLSCs group was higher than the other two groups at both 4 and 8 weeks after the operation (Fig. 6b). The results of hematoxylin-eosin (H & E) and Masson's trichrome staining are consistent with the micro-CT results, suggesting an efficient bone formation by GelMA + hPDLSCs (Fig. 7a, b). Similarly, ALP activity, which is generally used as a marker of osteoblast differentiation [35] shown in Fig. 7c was higher in GelMA and GelMA + hPDLSCs groups than in the control group. In particular, there was a large amount of dark brown staining in GelMA + hPDLSCs group, demonstrating higher ALP activity relative to the other samples. Overall, these results suggest that the GelMA hydrogel have greater ability to repair alveolar bone defects, which is further amplified when conjugated with hPDLSCs.

Our data suggest that the GelMA hydrogels-encapsulated hPDLSCs could offer an optimum physiochemical microenvironment to boost hPDLSCs adhesion and viability, which in turn may protect hPDLSCs from loss during the process of transplantation. Thus, GelMA hydrogels may be applied as stem cells carriers. The use of GelMA hydrogels-encapsulated hPDLSCs for therapy of alveolar bone defects may be a novel and promising way to facilitate alveolar bone regeneration.

5 Conclusion

In this work, we found that GelMA hydrogels in a liquid state could fill any irregular-shaped alveolar bone defect efficiently. Therefore, GelMA hydrogels can provide an appropriate physiochemical microenvironment for hPDLSCs adhesion, viability, osteogenic differentiation, which can protect hPDLSCs from being lost from a bone defect in the early stages of transplantation. Based on these principles, we investigated herein the potential of GelMA hydrogels-encapsulated hPDLSCs in alveolar bone regeneration. Our results showed that our proposed approach was efficient for the formation of new bone tissues in the alveolar bone defects, which received GelMA hydrogels with hPDLSCs. In comparison to controls and only GelMA hydrogels, significantly more bone volume was formed in the group treated with GelMA + hPDLSCs. The results described herein indicate that GelMA hydrogels-encapsulated hPDLSCs have a

significant alveolar regenerative potential. We believe these findings can pave the way for the design of new strategies for the therapy of alveolar bone defects.

Acknowledgements This work was supported by the National Natural Science Foundation of China (81470768, 21703031), Shanghai Science and Technology Innovation Fund (19ZR1445500), Project of Shanghai Municipal Health Commission (201840148) and Shanghai Talent Development Funding. JW thanks the funds from Donghua University for Distinguished Research Fellow.

Compliance with ethical standards

Conflict of interest The authors declare that they have no conflict of interest.

Publisher's note Springer Nature remains neutral with regard to jurisdictional claims in published maps and institutional affiliations.

References

1. Farré-Guasch E, Prins HJ, Overman JR, Ten Bruggenkate CM, Schulten EA, Helder MN, et al. Human maxillary sinus floor elevation as a model for bone regeneration enabling the application of one-step surgical procedures. Tissue Eng Part B Rev. 2013;19:69–82. https://doi.org/10.1089/ten.teb.2012.0404.
2. Du J, Mei S, Guo L, Su Y, Wang H, Liu Y, et al. Platelet-rich fibrin/aspirin complex promotes alveolar bone regeneration in periodontal defect in rats. J Periodontal Res. 2018;53:47–56. https://doi.org/10.1111/jre.12485.
3. Iviglia G, Cassinelli C, Torre E, Baino F, Morra M, Vitale-Brovarone C. Novel bioceramic-reinforced hydrogel for alveolar bone regeneration. Acta Biomater 2016;44:97–109. https://doi.org/10.1016/j.actbio.2016.08.012.
4. Akita D, Kano K, Saito-Tamura Y, Mashimo T, Sato-Shionome M, Tsurumachi N, et al. Use of rat mature adipocyte-derived dedifferentiated fat cells as a cell source for periodontal tissue regeneration. Front Physiol. 2016;7. https://doi.org/10.3389/fphys.2016.00050.
5. Han J, Menicanin D, Marino V, Ge S, Mrozik K, Gronthos S, et al. Assessment of the regenerative potential of allogeneic periodontal ligament stem cells in a rodent periodontal defect model. J Periodontal Res. 2014;49:333–45. https://doi.org/10.1111/jre.12111.
6. Yang Y, Rossi FM, Putnins EE. Periodontal regeneration using engineered bone marrow mesenchymal stromal cells. Biomaterials 2010;31:8574–82. https://doi.org/10.1016/j.biomaterials.2010.06.026.
7. Zhang L, Wang P, Mei S, Li C, Cai C, Ding Y. In vivo alveolar bone regeneration by bone marrow stem cells/fibrin glue composition. Arch Oral Biol. 2012;57:238–44. https://doi.org/10.1016/j.archoralbio.2011.08.025.
8. Fawzy El-Sayed KM, Mekhemar MK, Beck-Broichsitter BE, Bahr T, Hegab M, Receveur J, et al. Periodontal regeneration employing gingival margin-derived stem/progenitor cells in conjunction with IL-1ra-hydrogel synthetic extracellular matrix. J Clin Periodontol. 2015;42:448–57. https://doi.org/10.1111/jcpe.12401.
9. Seo B-M, Miura M, Gronthos S, Mark Bartold P, Batouli S, Brahim J, et al. Investigation of multipotent postnatal stem cells from human periodontal ligament. Lancet 2004;364:149–55. https://doi.org/10.1016/s0140-6736(04)16627-0.
10. Cantu DA, Hematti P, Kao WJ. Cell encapsulating biomaterial regulates mesenchymal stromal/stem cell differentiation and macrophage immunophenotype. Stem Cells Transl Med. 2012;1:740–9. https://doi.org/10.5966/sctm.2012-0061.
11. Moshaverinia A, Chen C, Xu X, Ansari S, Zadeh HH, Schricker SR, et al. Regulation of the stem cell-host immune system interplay using hydrogel coencapsulation system with an anti-inflammatory drug. Adv Funct Mater. 2015;25:2296–307. https://doi.org/10.1002/adfm.201500055.
12. Khayat A, Monteiro N, Smith EE, Pagni S, Zhang W, Khademhosseini A, et al. GelMA-Encapsulated hDPSCs and HUVECs for Dental Pulp Regeneration. J Dent Res. 2017;96:192–9. https://doi.org/10.1177/0022034516682005.
13. Nikkhah M, Eshak N, Zorlutuna P, Annabi N, Castello M, Kim K, et al. Directed endothelial cell morphogenesis in micropatterned gelatin methacrylate hydrogels. Biomaterials 2012;33:9009–18. https://doi.org/10.1016/j.biomaterials.2012.08.068.
14. Zhao X, Sun X, Yildirimer L, Lang Q, Lin ZYW, Zheng R, et al. Cell infiltrative hydrogel fibrous scaffolds for accelerated wound healing. Acta Biomater 2017;49:66–77. https://doi.org/10.1016/j.actbio.2016.11.017.
15. Annabi N, Tamayol A, Uquillas JA, Akbari M, Bertassoni LE, Cha C, et al. 25th anniversary article: Rational design and applications of hydrogels in regenerative medicine. Adv Mater 2014;26:85–123. https://doi.org/10.1002/adma.201303233.
16. Nichol JW, Koshy ST, Bae H, Hwang CM, Yamanlar S, Khademhosseini A. Cell-laden microengineered gelatin methacrylate hydrogels. Biomaterials 2010;31:5536–44. https://doi.org/10.1016/j.biomaterials.2010.03.064.
17. Chen YC, Lin RZ, Qi H, Yang Y, Bae H, Melero-Martin JM, et al. Functional human vascular network generated in photocrosslinkable gelatin methacrylate hydrogels. Adv Funct Mater. 2012;22:2027–39. https://doi.org/10.1002/adfm.201101662.
18. Yue K, Trujillo-de Santiago G, Alvarez MM, Tamayol A, Annabi N, Khademhosseini A. Synthesis, properties, and biomedical applications of gelatin methacryloyl (GelMA) hydrogels. Biomaterials. 2015;73:254–71. https://doi.org/10.1016/j.biomaterials.2015.08.045.
19. Fairbanks BD, Schwartz MP, Bowman CN, Anseth KS. Photoinitiated polymerization of PEG-diacrylate with lithium phenyl-2,4,6-trimethylbenzoylphosphinate: polymerization rate and cytocompatibility. Biomaterials 2009;30:6702–7. https://doi.org/10.1016/j.biomaterials.2009.08.055.
20. Zhao BJ, Liu YH. Simvastatin induces the osteogenic differentiation of human periodontal ligament stem cells. Fundam Clin Pharm. 2014;28:583–92. https://doi.org/10.1111/fcp.12050.
21. Koh KS, Choi JW, Park EJ, Oh TS. Bone regeneration using silk hydroxyapatite hybrid composite in a rat alveolar defect model. Int J Med Sci. 2018;15:59–68. https://doi.org/10.7150/ijms.21787.
22. Nguyen PD, Lin CD, Allori AC, Ricci JL, Saadeh PB, Warren SM. Establishment of a critical-sized alveolar defect in the rat: a model for human gingivoperiosteoplasty. Plast Reconstructive Surg. 2009;123:817–25. https://doi.org/10.1097/PRS.0b013e31819ba2f4.
23. Nguyen PD, Lin CD, Allori AC, Schachar JS, Ricci JL, Saadeh PB, et al. Scaffold-based rhBMP-2 therapy in a rat alveolar defect model: implications for human gingivoperiosteoplasty. Plast Reconstr Surg. 2009;124:1829–39. https://doi.org/10.1097/PRS.0b013e3181bf8024.
24. Lee JS, Kim E, Han S, Kang KL, Heo JS. Evaluating the oxysterol combination of 22(S)-hydroxycholesterol and 20(S)-hydroxycholesterol in periodontal regeneration using periodontal ligament stem cells and alveolar bone healing models. Stem Cell Res Ther. 2017;8:276. https://doi.org/10.1186/s13287-017-0725-9.
25. Su F, Liu SS, Ma JL, Wang DS, E LL, Liu HC. Enhancement of periodontal tissue regeneration by transplantation of osteoprotegerin-engineered periodontal ligament stem cells. Stem Cell Res Ther. 2015;6:22. https://doi.org/10.1186/s13287-015-0023-3.
26. Wada N, Menicanin D, Shi S, Bartold PM, Gronthos S. Immunomodulatory properties of human periodontal ligament stem

cells. J Cell Physiol. 2009;219:667–76. https://doi.org/10.1002/jcp.21710.
27. Alge DL, Anseth KS. Bioactive hydrogels: Lighting the way. Nat Mater 2013;12:950–2. https://doi.org/10.1038/nmat3794.
28. West JL. Protein-patterned hydrogels: customized cell microenvironments. Nat Mater 2011;10:727–9. https://doi.org/10.1038/nmat3132.
29. Monteiro N, Thrivikraman G, Athirasala A, Tahayeri A, Franca CM, Ferracane JL, et al. Photopolymerization of cell-laden gelatin methacryloyl hydrogels using a dental curing light for regenerative dentistry. Dent Mater 2018;34:389–99. https://doi.org/10.1016/j.dental.2017.11.020.
30. Liu Y, Chan-Park MB. A biomimetic hydrogel based on methacrylated dextran-graft-lysine and gelatin for 3D smooth muscle cell culture. Biomaterials 2010;31:1158–70. https://doi.org/10.1016/j.biomaterials.2009.10.040.
31. Hu J, Hou Y, Park H, Choi B, Hou S, Chung A, et al. Visible light crosslinkable chitosan hydrogels for tissue engineering. Acta Biomater 2012;8:1730–8. https://doi.org/10.1016/j.actbio.2012.01.029.
32. Shin SR, Aghaei-Ghareh-Bolagh B, Dang TT, Topkaya SN, Gao X, Yang SY, et al. Cell-laden microengineered and mechanically tunable hybrid hydrogels of gelatin and graphene oxide. Adv Mater 2013;25:6385–91. https://doi.org/10.1002/adma.201301082.
33. Celikkin N, Mastrogiacomo S, Jaroszewicz J, Walboomers XF, Swieszkowski W. Gelatin methacrylate scaffold for bone tissue engineering: the influence of polymer concentration. J Biomed Mater Res A 2018;106:201–9. https://doi.org/10.1002/jbm.a.36226.
34. Miri AK, Hosseinabadi HG, Cecen B, Hassan S, Zhang YS. Permeability mapping of gelatin methacryloyl hydrogels. Acta Biomater 2018;77:38–47. https://doi.org/10.1016/j.actbio.2018.07.006.
35. Pan J, Wang J, Hao L, Zhu G, Nguyen DN, Li Q, et al. The triple functions of D2 silencing in treatment of periapical disease. J Endod 2017;43:272–8. https://doi.org/10.1016/j.joen.2016.07.014.